

Modeling of Field Distribution and Energy Storage in Diphasic Dielectrics

S. K. Patil, M. Y. Koledintseva, and R. W. Schwartz
Missouri University of Science and Technology, Rolla, MO, 65409, USA

Modeling of electrostatic field distribution and energy storage in diphasic dielectrics containing high-permittivity BaTiO₃ in a glass host has been carried out analytically and numerically. An analytical formulation employs the Maxwell Garnett (MG) mixing rule, and numerical simulation uses software based on the boundary element method (BEM). The field distribution was studied as a function of a dielectric contrast and a volume fraction of phases. For a high-permittivity sphere enclosed in a low-permittivity glass cube it was found that the dielectric contrast of 75 and volume fraction of 46.8% led to the increased energy storage density. For composites with lower volume fractions of high-permittivity inclusions, the field enhancement factor of 2.6 was observed, whereas for the higher volume-fraction composites, field enhancement up to 10 was noticed. The higher field enhancement factors are expected to lead to dielectric breakdown at the lower applied fields, limiting energy density. The upper limit of applicability of the MG formulation in terms of the inclusion volume fraction was also established, and it is a function of the dielectric contrast. The host material permittivity causes a substantial variation in the applicability limit of the MG mixing rule, while the permittivity of inclusion phase does not affect the limit.

Keywords: Dielectric composites, electric field distribution, energy storage

I. INTRODUCTION

The properties of dielectric mixtures have been investigated for more than 100 years.¹⁻⁵ One of the objectives of the research in this area has been the development of dielectric bodies with enhanced energy storage capabilities, for example, crystallization of a phase with higher permittivity, like BaTiO₃, in a glass matrix.⁶ The general goal is to take advantages of both high energy storage capacity of the BaTiO₃ inclusions and high breakdown strength of the glass phase. This approach may eliminate the porosity that causes field concentration (enhancement) adversely impacting breakdown.⁷ Other ways of solving this problem are based on the dispersing materials with high permittivities, such as BaTiO₃, into polymeric hosts to assure high energy density, high breakdown strength, low dielectric loss, fast speed, low cost, and graceful failure leading to higher reliability.^{8,9} Recent studies of these composites have resulted in effective permittivities between 20 and 115,¹⁰⁻¹¹ depending on the volume fraction of a filler and attributes of the synthesis process.

The dielectric response of such composites has been modeled using different effective medium theories.¹²⁻¹⁶

Description of the dielectric behavior of these materials is based on formulations that include the dielectric properties of two constituent phases and their volume fractions. The geometry of inclusions is also important, and typically, ellipsoidal inclusions are assumed.¹⁷⁻¹⁸ Energy storage characteristics of a composite material may be found knowing effective permittivity retrieved using a quasistatic approximation. This means that the size of the inclusions is much smaller than the wavelength in the medium. Also, the materials are assumed to be linear.

It has been reported that Maxwell Garnett (MG) formulation for diphasic dielectrics can be applied up to 30 % volume fraction of inclusions, that is, for comparatively dilute mixtures.¹⁹ Most known mixing rules assume that the lines of electric flux are *not distorted* by the particles, and hence, there are inherent limitations in accurately predicting the energy storage capabilities of composites.²⁰ For heterogeneous composite the electric lines of flux will tend to distribute them according to the permittivity ratios of the host and the inclusion phase.²¹ Local inhomogeneities in electric field distribution, *i.e.*, field enhancement in the low permittivity phase and field penetration in the high permittivity (ϵ) phase, are not taken into account by classical mixing theories.

Numerical simulation results demonstrate that the electric field distribution in composites may be of three different types. The first type is the field enhancement in the low-permittivity phase at the boundary separating two phases in the direction of the applied field. The second type is the field in high permittivity phase – this is a low-intensity field. The third type is the intermediate-intensity field in the low permittivity phase. An insightful study to understand field distribution in such composites was carried out, but it is limited only by two-dimensional cases.²²

The present study is aimed at a comprehensive analysis of the impact of the field distribution on the energy storage and breakdown strength. To do this, it is necessary to quantify electric field distribution and gain a profound understanding of the parameters that determine this distribution. For solving this problem, the dielectric properties of constituent phases and their volume fractions should be determined. This specifically involves identifying an ideal *dielectric contrast*. The dielectric contrast is defined as the ratio of the permittivity of the inclusion phase to the permittivity of the host phase:

$$c = \frac{\epsilon_{incl}}{\epsilon_{host}}, \quad (1)$$

The three-dimensional (3D) numerical simulation software (*Coulomb*) is used in the present study to comprehensively analyze an impact of the field distribution on the energy storage and breakdown strength. This software is based on the solution of the Laplace's electrostatic equation and allows for taking into account local inhomogeneities in the field distribution. The results of simulations are interpreted from the perspectives of field enhancement and field penetration into the high permittivity phase. One of the important questions to be answered is how these properties are related to the dielectric breakdown.

Another goal of this work is to determine the limits of applicability of the Maxwell Garnett formulation in terms of the inclusion volume fraction. Maxwell Garnett theory has been accepted as a satisfactory approximation, when inter-particle interactions and multiple scattering are not significant, *i.e.*, when there are dilute mixtures.²³ Though scientific community has been cognizant of this limitation, the minimum limit on the inclusion volume fraction (or inter-inclusion separation distance) has not been established yet.

Herein, the results for diphasic dielectric bodies with different permittivities and volume fractions are reported. A three-dimensional model of a composite is based on a sphere enclosed in a cube (SEC), with the cube representing a low-permittivity (*e.g.*, glass) phase, and a spherical inclusion representing a high-permittivity (*e.g.*, barium titanate) phase. It needs to be mentioned here that the assumption of a sphere enclosed in a cube matrix is a special "non-random" case. V. Myroshnychenko *et. al* have rightfully acknowledged the fact that in spite of earnest computational advances and ability to model randomly dispersed inclusions, as well as non-random structures, it has been difficult to find experimental systems that bear close resemblance to the idealized models.²⁴ V. Myroshnychenko *et. al.* have developed an algorithm for 2D case with random inclusions for two cases of surface fractions: percolating systems and non-percolating systems, and compared their results with other traditional EMT theories. However, local electric field distribution as a function of inclusion volume fraction and dielectric contrast has not explored. Herein, the electric field increase has been quantified as a function of the properties of the inclusion and the host phase. The MG formulation was also applied to calculating effective permittivity of this system, and the results of the two approaches are compared.

II. SIMULATIONS

A. METHOD AND SOFTWARE FOR NUMERICAL SIMULATIONS

Simulations were carried out using the commercially available software *Coulomb* from Integrated Engineering Software (Winnipeg, Manitoba, Canada). *Coulomb* is a 3D code that uses a boundary element method to solve Laplace's equation for electrostatic potential inside the geometry of interest.^{26,27} Laplace's equation

$$\nabla^2 V = 0 \quad (2)$$

is a particular case of the Poisson's equation,

$$\nabla^2 V = -\frac{q_{vol}}{\epsilon}, \quad (3)$$

where q_{vol} is the free charge volume density, V is the electric potential, and $\epsilon = \epsilon_0 \epsilon_r$ is the permittivity of the medium.

Compared to finite element methods (FEM) and finite difference methods (FDM), the boundary element method reduces the number of calculations that must be performed for the solution of electrostatic potential problems. Automatic grid functions are available within this package, and they have been used in the present research to define the boundary grid.

Coulomb allows for the construction of the larger 3D structures containing periodically repeated cells with identical properties to represent uniform diphasic dielectrics. It should also be noted that the dielectric behavior of the composite can also be obtained through studying a single cell. Fig. 1 shows a cell with a "sphere enclosed in a cube" (SEC) geometry and its 3-D translation in x , y , and z directions.

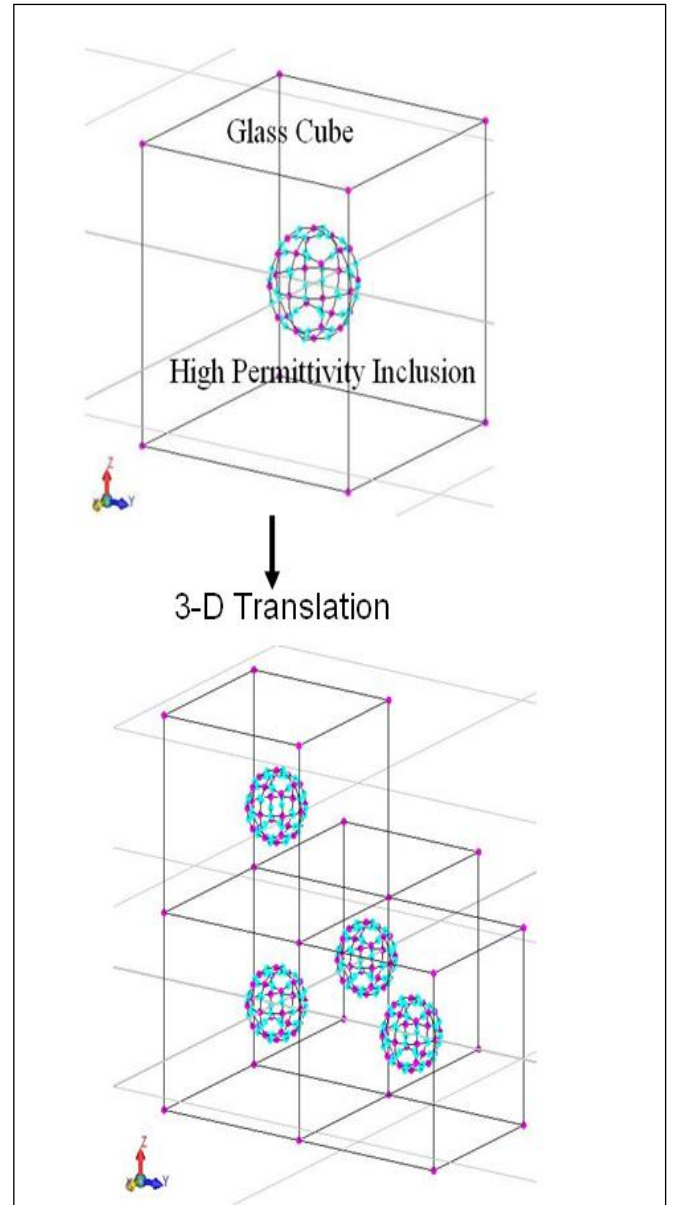


FIG. 1. Basic building block of composite sphere enclosed in cube and 3-D translation in x , y , z directions.

Simulations using *Coulomb* were run to understand local field distribution as a function of inclusion volume fraction and its impact on the energy stored in the composite. In these simulations, the applied electric field was $E_{appl} = 50$ kV/cm, the host phase was assigned a permittivity $\epsilon_{r,host}$ ranging from 4 to 100, and the inclusion ‘high-permittivity’ phase was assigned a permittivity $\epsilon_{r,incl}$ from 600 to 1200. The simulated dielectric body was a $9 \times 9 \times 9$ matrix of cubes (1.1 μm edge length/cube) and included 729 inclusion spheres. The linear periodic simulation function of the *Coulomb* code was used to create the dielectric body. The inclusion volume fraction varied from approximately 1 to 50 % by varying the radius of the spherical inclusions from 0.2 μm to 0.53 μm . Energy density predictions of *Coulomb* were compared with the MG results for inclusion volume fractions up to 30%.

The *Coulomb* software was also used to simulate the impact of the permittivity of the host phase on the field enhancement within that phase. Studies in this area are of interest since field enhancement can affect breakdown strength. The effects of dielectric contrast were studied by adopting two strategies: (1) varying the permittivity of host phase, and (2) varying the permittivities of both host and inclusion phases. Simulations were also carried out to map field penetration into the high-permittivity phase, since this can result in higher energy storage densities.

The results are presented below in Section III.

B. Maxwell Garnett mixing rule

The Maxwell Garnett (MG) formulation has historically been the simplest and the most popular mixing rule for homogenizing particulate composite media. Homogenization of a mixture is used in the quasistatic approximation, when sources and fields are varying slowly. This demands that the characteristic size of scattering particles or correlation distance (in the case of the medium is described by continuous permittivity function) is small compared to wavelength in the effective medium.²⁸ In addition, a mixture should be sparse, and inter-particle distances are big enough, so that multiple scattering is negligible.^{17, 28}

The MG rule for a mixture of a base material with relative permittivity ϵ_b and spherical inclusions with relative permittivity ϵ_s as given by^{1, 17}:

$$\epsilon_{eff} \cong \epsilon_{r,host} + \frac{3f_{incl}\epsilon_{r,host}(\epsilon_{r,incl} - \epsilon_{r,host})/(\epsilon_{r,incl} + 2\epsilon_{r,host})}{1 - f_{incl}(\epsilon_{r,incl} - \epsilon_{r,host})/(\epsilon_{r,incl} + 2\epsilon_{r,host})}, \quad (4)$$

The electric energy stored within an elemental volume (energy density) is a function of the effective permittivity ϵ_{eff} and the square of the applied electric field E :

$$w = \frac{1}{2} \epsilon_0 \epsilon_{eff} E_{appl}^2. \quad (5)$$

The energy density calculated this way is compared with the energy density extracted from the

Coulomb simulations. The comparison results are presented in Section III.

III. RESULTS AND DISCUSSION

A. FIELD BEHAVIOR IN COMPOSITES WITH DISPERSED INCLUSIONS

The effect of particle size on field distribution within the composite dielectric was studied. The electric field distribution over the cross-section for different size of inclusion spheres of a single cell is shown in Fig. 2 (a, b). The inclusion particle in Fig. 2 (a) has the diameter of 0.4 μm , and the particle in Fig. 2 (b) has the diameter of 0.8 μm . The single cell is translated in three directions to form the $9 \times 9 \times 9$ dielectric body. An electric field magnitude may be estimated by using the color scale on the left hand side of each figure. The most important result is that the field magnitude within the high permittivity particles is greatly reduced compared to the magnitude of the applied field. If the permittivity of the inclusion phase is 1200, the host phase permittivity is 4, and the applied electric field is 50 kV/cm, the field magnitude within the particle is below 5 kV/cm. This suggests that, despite the high permittivity of the inclusion phase, the energy storage density of this phase is greatly reduced due to minimal field penetration into the phase. This result agrees with the prior reports of limited energy storage characteristics for composite materials prepared from polymers and high permittivity inclusions.²⁵

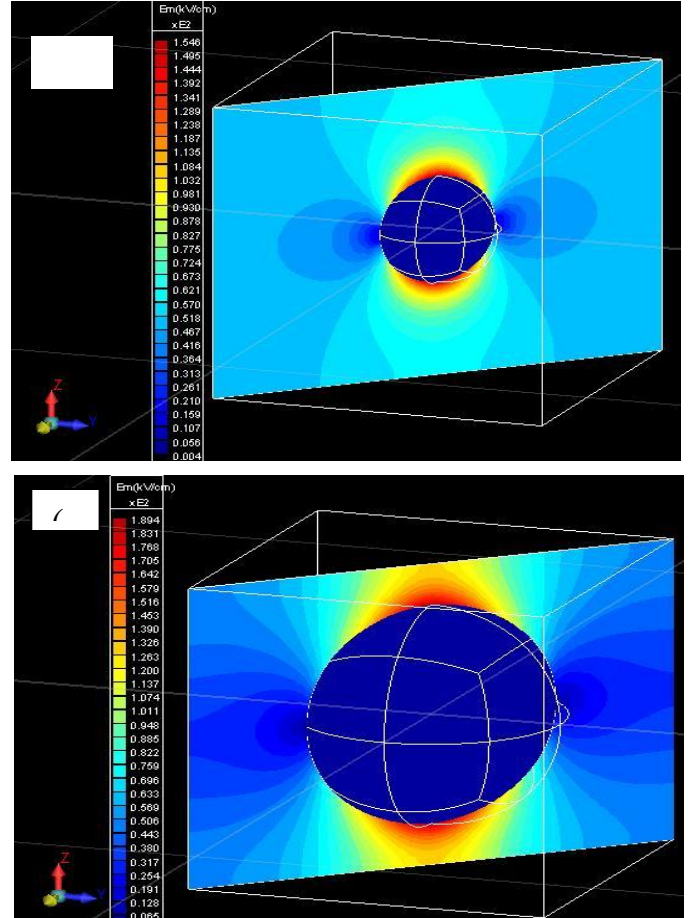


FIG. 2. Electric field distribution in the composite in the host low-permittivity phase and in the spherical high-permittivity inclusion phase: (a) low volume fraction of the inclusion (2.5 %); (b) high volume fraction of the inclusion (20.1 %).

Other characteristics of the field distribution in both composites (Fig. 2 (a) and (b)) are similar, though the magnitude and extent of the field enhancement in the host phase depends on the particle size of the high-permittivity inclusion. Composites prepared with the particles of the smaller diameter exhibit a lower field enhancement compared to the particles of larger diameter.

Smaller inclusion size and the proximity of the high-permittivity inclusions to each other can have a significant impact on the field *enhancement factor*. The enhancement factor is defined as the ratio of the maximum field present in the composite to the magnitude of the applied field.

$$F_e = \frac{E_{\max}}{E_{\text{appl}}} \quad (5)$$

The field enhancement for the 0.4- μm particle composite is approximately $F_e = 3.1$, while the field enhancement factor for the 0.8- μm particle composite is approximately $F_e = 3.8$. Other notable differences are that for the 0.4- μm particle composite, a field slightly greater than the applied field exists at most locations within the matrix phase, as indicated by the light blue color representing a field of $E \sim 60$ kV/cm. Other locations in the matrix exhibit a field of magnitude that is approximately equal to the applied field (next field gradation color of blue, $E \sim 49.8$ kV/cm).

The similar result is observed for the composite prepared from the 0.8- μm particle, though the specifics of the field distribution are noticeably different. For this composite, the significant field enhancement also extends to the cell border (in the field direction), albeit in a more localized fashion than for the 0.4- μm particle composite.

It should be mentioned that the field penetration, field enhancement, and field distribution characteristics are all the functions of not only volume fraction, as the particular case considered above demonstrates, but dielectric contrast as well. This will be shown below.

B. EFFECTS OF INCLUSION VOLUME FRACTION AND DIELECTRIC CONTRAST ON LOCAL FIELD DISTRIBUTION

This section contains quantitative results that show the effect of the dielectric contrast on both the field penetration in a high-permittivity region and the field enhancement. To the best of our knowledge, no quantitative estimates have been reported so far.

Field distribution inside a composite has three main regions, as described earlier. The first region has the enhanced field in the low-permittivity phase at the boundary separating two phases in the direction of the applied field, see the top and the bottom of the inclusion spheres in Fig. 2 (a, b). The second region is the low-intensity field in high permittivity phase, namely, inside the inclusion spheres. The third region is the intermediate-intensity field in the low permittivity phase, everywhere, except for the first region. The enhancement of the field in the first region is an important parameter that affects the breakdown strength of the composite. The higher field penetration into the high-permittivity inclusion (represented

as the second region of field) will lead to the higher energy storage densities. It is critical to develop insights into field enhancement and field penetration that are the functions of the inclusion volume fraction f_{incl} and the dielectric contrast c . These insights would help in developing guiding principles for engineering dielectrics for high-energy capacitors.

Fig. 3 illustrates how the properties of the two phases and the size of the inclusion can impact the field enhancement within the composite. According to Fig. 3, for the smallest inclusions (0.2 μm radius), the field enhancement factor is about $F_e = 2.6$. In contrast, for larger inclusions (0.53 μm radius), the field enhancement factors $F_e > 10$ are observed. Thus, in a system with the inclusion permittivity $\epsilon_{\text{incl}} = 1200$ and the host permittivity $\epsilon_{\text{host}} = 4$, the local field in the vicinity of an inclusion can vary from ~ 140 kV/cm to ~ 600 kV/cm, when the applied field is 50 kV/cm.

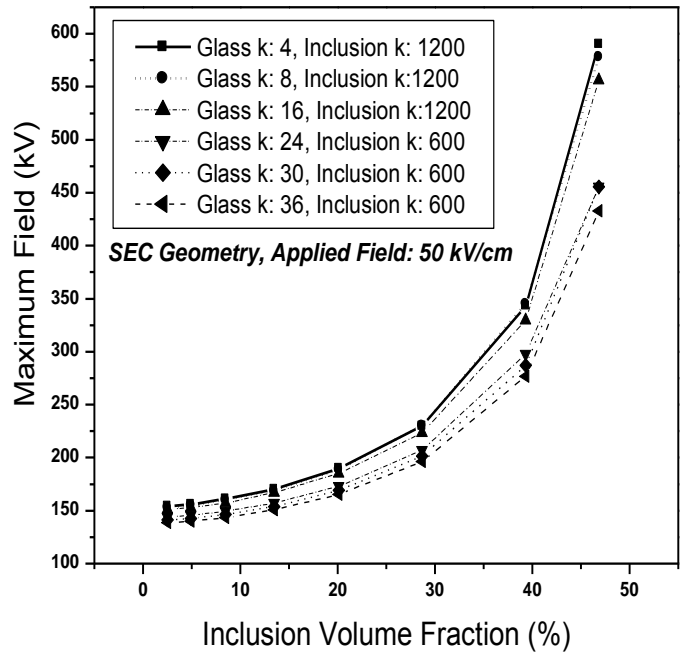


FIG. 3. Coulomb simulations of the maximum field in the host material as a function of the inclusion volume fraction (%).

The impact of the “dielectric contrast” on the field enhancement may be also seen in Fig. 3. Based on the permittivities of the two phases, the dielectric contrast was varied from approximately 16 ($\epsilon_{\text{host}} = 36$ and $\epsilon_{\text{incl}} = 600$) to 300 ($\epsilon_{\text{host}} = 4$ and $\epsilon_{\text{incl}} = 1200$). As a particular case of a diphasic dielectric, a glass ceramic system, consisting of barium titanate inclusions in glass matrix is considered. Glass is the low permittivity phase. If the permittivity of the glass phase increases (36 vs. 4), the field enhancement factor reduces by approximately 25%. Because there is likely a strong link between the dielectric breakdown strength and the field enhancement, this result suggests that the ability to develop residual glass phases with higher permittivities (assuring the lower dielectric contrast with inclusions) can be beneficial in improving the breakdown characteristics of composites.

Fig. 4 shows the field penetration that takes place along the z-axis, when the electric field of 50 kV/cm is applied in the z-direction. It is interesting to decouple the volume fraction and dielectric contrast effect from the Fig. 4. For a dielectric contrast of 300 and increase in volume fraction from 2.5 to 46.8 %, there is 17 times increase in the maximum field that has penetrated. However, with a dielectric contrast of 16 and for the same increase in volume fraction the maximum field penetrated increases 3.25 times. Also, for a constant volume fraction of 2.51 % and dielectric contrast varying from 300 to 16, it is seen that the maximum field penetration has increased almost 13 times. Considering the case for constant volume fraction of 46.84 % and for the same change in the dielectric contrast, maximum field penetrated has increased 2.5 times. These results are revealing very important information about volume fraction and dielectric contrast effects. Important observation is that for higher dielectric contrast, increase in volume fraction of the high permittivity phase will lead to higher field penetration. Also, it should be noticed that as the dielectric contrast decreases, the maximum field penetration at lower concentrations of inclusions is higher than at higher concentrations. It is seen from these simulations that the significant field penetration into a high-permittivity inclusion occurs only when the dielectric contrast is reduced below approximately 75. Fig. 4 also shows that the field penetration into the inclusion can increase when the volume fraction of the high permittivity phase increases. These results are important for the design of high energy density composites, since significant field penetration into the high-permittivity phase is required to achieve high energy density values. These quantitative results clarify the role that the properties of the phases and microstructural characteristics can exert on local field behavior within the dielectric.

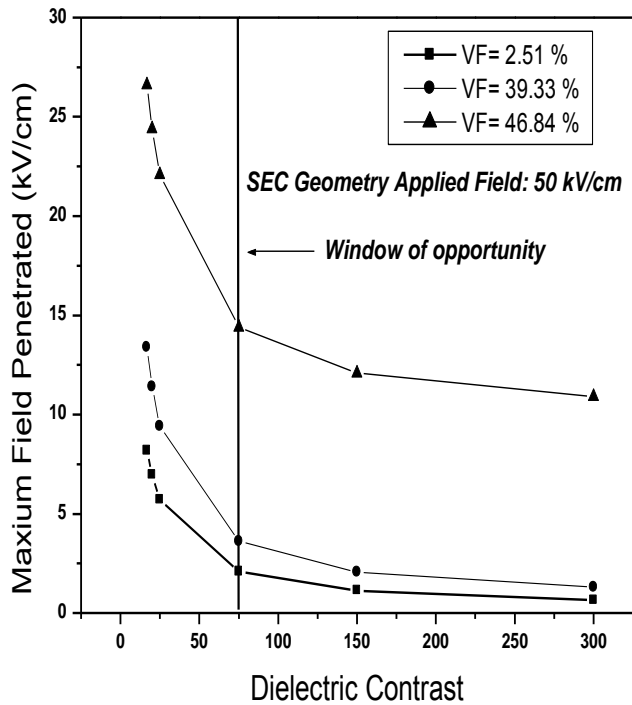


FIG. 4. *Coulomb* simulations of the maximum field present in a high-permittivity spherical inclusion enclosed in the glass matrix as a function of dielectric contrast for different inclusion volume fractions.

C. BENCHMARKING OF ENERGY STORAGE CALCULATIONS

Consider a single-phase dielectric (glass $\epsilon = 41$) cube with a side of $1.1 \mu\text{m}$, as is shown in Fig. 5 (a). In our computations, the electric field applied in the vertical direction of the cube is assumed to be 81 kV/mm. We used the same value of electric field as in the experiments carried out in Penn State University⁶. We calculated energy storage within glass using the software *Coulomb*. The cube in this example is subdivided into 1000 tetrahedral elements to increase the accuracy of simulations. *Coulomb* predicts energy stored within the cube of $1.55 \cdot 10^{-12} \text{ J}$, which corresponds to the energy density of 1.16 J/cm^3 . These results match with those obtained at Penn State University⁶: the experimentally predicted energy storage for glass with permittivity of 40 was also 1.16 J/cm^3 , as is shown in Fig. 5(b).

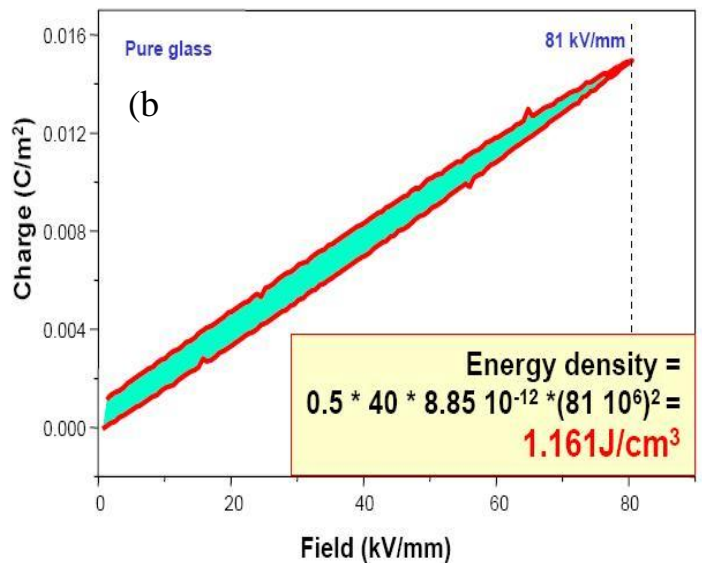
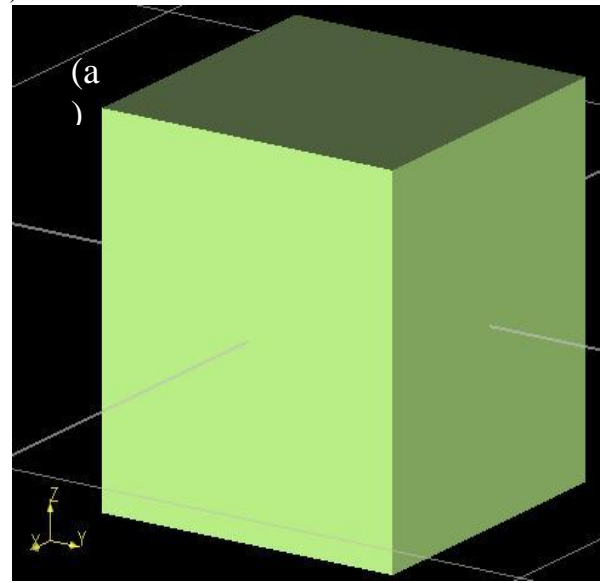


FIG. 5. (a) 3D cube, generated in *Coulomb*, representing pure glass phase; (b) Experimentally obtained energy storage in the pure glass phase system.

Though the results of computations and experiments agree well for a single-phase system, it is

immensely difficult to compare predictions for diphasic systems. *Coulomb* is well-suited for ordered non-random composites. However, it is extremely difficult to reproduce the realistic irregular (non-periodic) grain structure in *Coulomb*.

D. COMPARISON OF COULOMB AND MAXWELL GARNETT MODELS

One of the primary limitations of mixing theories is inability to predict energy density beyond a particular limit of the inclusion volume fraction, as was discussed in Section 2.2. According our knowledge, a precise limit at which mixing theories correctly take into account field enhancement and penetration has not been established. This is a topic of the present investigation.

Maxwell Garnett theory was applied to the same models developed in *Coulomb* for different volume fractions of inclusions. The host matrix is assumed to be glass with different permittivities. The inclusions are spheres with permittivity of 1200. The effective permittivity obtained using MG formula (4) as a function of the volume fraction at different values of the host permittivity is plotted in Fig. 6. As seen from the plot, the effective permittivity increases significantly with the increase of the host permittivity.

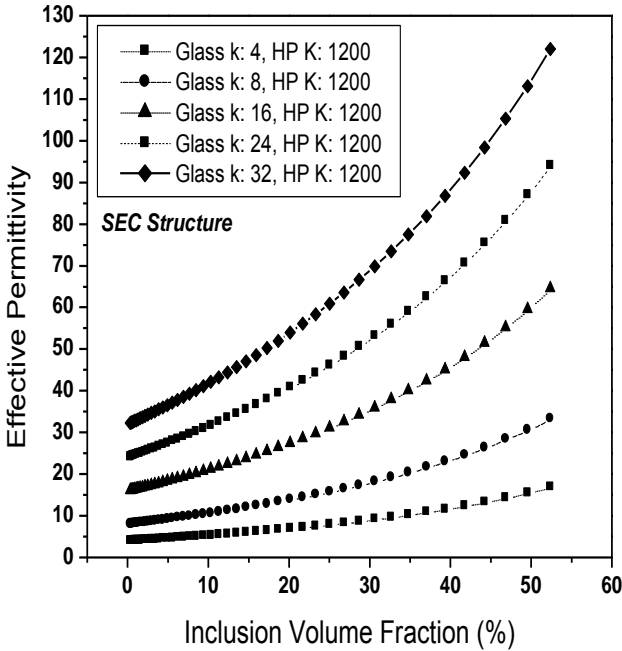


FIG. 6. MG prediction of effective permittivity for a sphere enclosed in cube as a function of volume fraction for different values of host permittivity

The energy storage can be easily calculated using (5), if the effective permittivity is known. The energy density for the SEC structure was calculated up to the inclusion volume fraction of 30 % using both *Coulomb* and the MG model. It was noted that the deviation between the *Coulomb* and the MG predictions occurs at very low volume fractions of inclusions. It is convenient to introduce a criterion on how well the MG and *Coulomb* results agree,

$$p = \frac{|E_{MG} - E_{Coulomb}|}{E_{av}} \cdot 100\%, \quad (6)$$

where $E_{av} = \frac{E_{MG} + E_{Coulomb}}{2}$ is the average energy stored in the cube with a sphere, calculated through both the MG model and *Coulomb* software.

Herein, it was assumed that the $p > 10\%$ discrepancy between the MG and *Coulomb* is a significant difference between the two approaches. Fig. 7 shows a plot of discrepancy p (in %) between the MG and *Coulomb* as a function of the volume fraction f_{incl} for the SEC structure. The applied field is 50 kV/cm. When the dielectric contrast is 300, the significant discrepancy between the MG and *Coulomb* (more than 10 %) occurs at the volume fraction of inclusions $f_{incl} > 4\%$. This is the volume fraction limit denoted as f_{lim} . The value f_{lim} shifts to about 5.5%, when the dielectric contrast c reduces to 16. The value f_{lim} shifts to around 7%, when the dielectric contrast c is further decreased to 6. Thus, Fig. 7 demonstrates that the volume fraction limit f_{lim} increases as the dielectric contrast decreases. This means that the smaller the difference between the permittivities of the two phases, the higher volume fraction up to which the MG formulation can be applied.

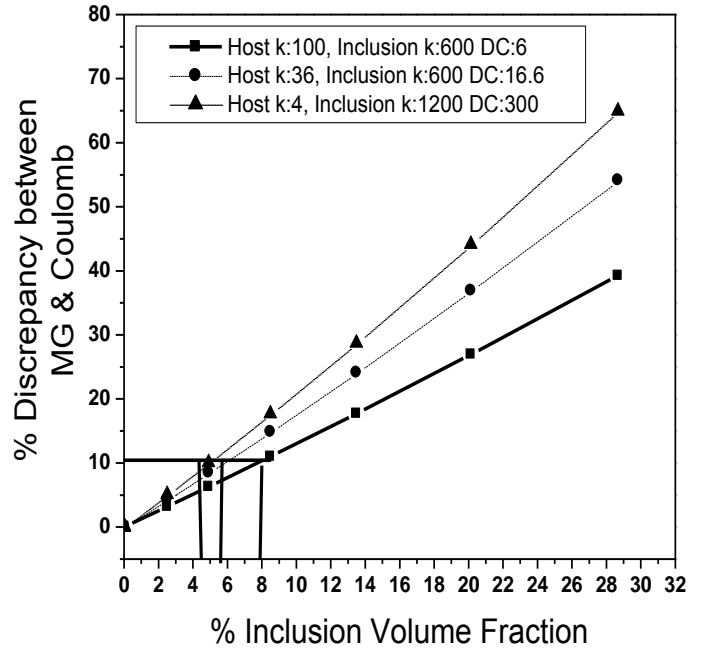


FIG. 7. Discrepancy between MG and *Coulomb* predictions as a function of inclusion volume fraction. The dielectric contrast is varied by varying both host and inclusion permittivity.

Two sets of simulations were run to determine the effect of permittivities of the inclusion and host phases on the inclusion volume fraction limit f_{lim} . First, the permittivity of the inclusion was varied, while the host permittivity remained the same. Second, the host permittivity was varied, while the inclusion permittivity was kept constant. Fig. 8 shows the discrepancy between the MG model and *Coulomb*. It may be seen that there is a substantial difference in the inclusion volume fraction limit, when only the permittivity of the host is varied. This

suggests that the volume fraction limit for applicability of the MG formalism varies from approximately 5 to 8%.

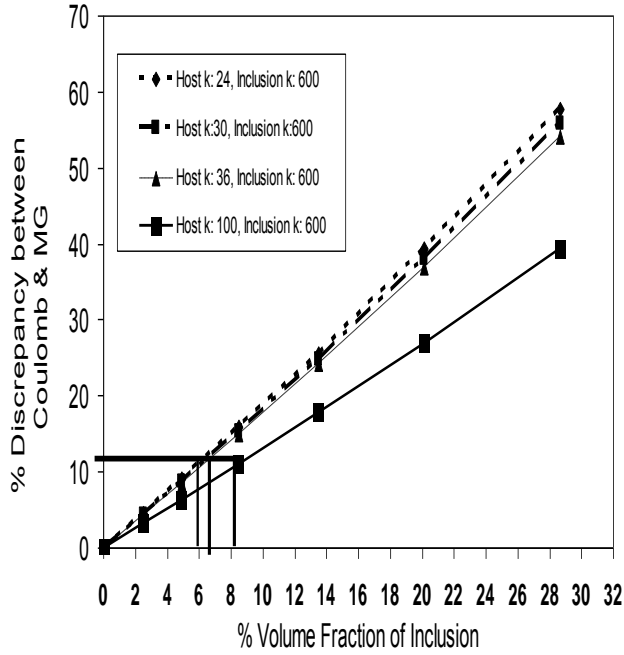


FIG. 8. Discrepancy between the MG and *Coulomb* predictions as a function of the inclusion volume fraction. The dielectric contrast is varied by varying only host permittivity (inclusion permittivity is constant).

Fig. 9 shows that when the inclusion permittivity varies, there is *almost no effect* upon the inclusion volume fraction limit f_{lim} . Thus, the volume fraction limit definitely depends on the dielectric contrast; however, it is the host permittivity that plays the crucial part in governing this limit.

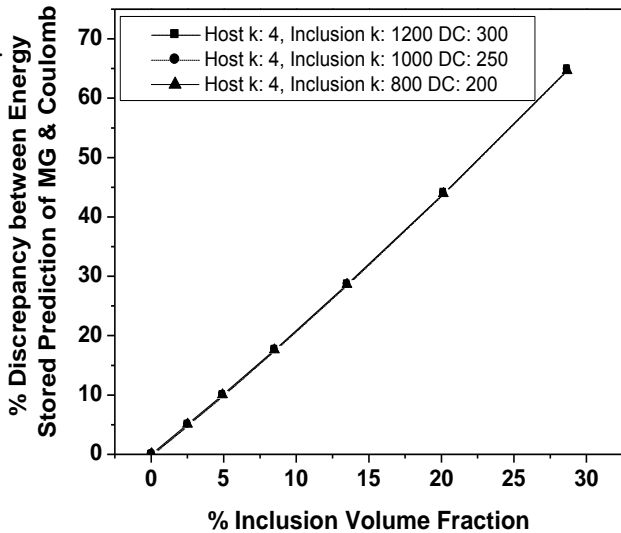


FIG. 9. Discrepancy between the MG and *Coulomb* predictions as a function of volume fraction of inclusions. The dielectric contrast is varied by varying only inclusion permittivity (host permittivity is constant).

It is important to mention that though this inclusion volume fraction limit has been estimated for the first time, there are other ways to extend applicability limit of the MG theory. For example, there is an incremental MG model

proposed by A. Lahtakia¹⁹, where the inclusion phase is always dilute, and it is added incrementally to the new homogenized host at every iteration cycle. The resultant effective permittivity converged to the result predicted by Bruggeman's formula.²⁹ Another approach is described in A. Sihvola's paper,²⁸ where the ν -parameter is introduced to take into account the interaction of polarizations of neighboring inclusions, when calculating the dipole moment of a single scatterer. The parameter $\nu = 0$ corresponds to the MG formulation; $\nu = 2$ corresponds to the Bruggeman's formula, and $\nu = 3$ gives the CP ("Coherent Potential") formula.^{30, 31} The discrepancy between the MG ($\nu = 0$) and the other mixing rules ($\nu = 1, 2, 3$) starts to be noticeable, when the inclusion volume fraction is around 10% [30, Fig. 3]. The dielectric contrast in these computations appears to be very low. Our comparison of the MG formulation with *Coulomb* numerical modeling yields the limit from 4 to 8%, depending on the dielectric contrast ($c = 16 - 300$), which reasonably agrees with the results in papers.^{30, 31}

IV. CONCLUSIONS

Modeling of electrostatic field distribution and energy storage in diphasic dielectrics containing high-permittivity BaTiO₃ in a glass host material have been studied using numerical simulations using software *Coulomb* and an analytical modeling based on the Maxwell Garnett mixing rule. Studies focused on a dielectric structure consisting of a cube of low permittivity phase (glass or polymer) and isotropic spherical inclusion representing high permittivity inclusion phase (ceramic, e.g., BaTiO₃). Using *Coulomb*, it is found that the field distribution inside a structure can be subdivided into three regions: (1) the field enhancement that takes place as the electric field lines encounter a sharp discontinuity in permittivity across a diphasic interface; (2) low-intensity field penetration into the high permittivity phase; and (3) intermediate-intensity field inside the low-permittivity region. The first region is where the breakdown might happen, so it determines the breakdown strength of the composite. The field in the second region depends on the dielectric contrast of the composite, and it determines the highest possible energy storage density.

This research has resulted in quantification of the field enhancement and field penetration. The field distribution was studied as a function of the dielectric contrast and volume fraction of the inclusion phase. For the geometry with a high-permittivity barium titanate sphere enclosed in a low-permittivity glass cube, it was found that the dielectric contrast of 75 and volume fraction of 46.8% lead to the enhanced field penetration into the high permittivity phase, which allows for increasing energy density stored within the composite, assuming that the breakdown behavior can be effectively optimized.

These results suggest opportunities for microstructural and compositional engineering to achieve high energy density dielectrics. For composites with lower inclusion volume fractions, a field enhancement factor of 2.6 was observed, whereas for higher volume fraction composites, a field enhancement of 10 was observed. The higher the field enhancement factor, the higher the probability of electric breakdown.

The upper limit of applicability of the MG formulation in terms of the inclusion volume fraction was also investigated. This limit depends on the dielectric contrast. It was found that as the dielectric contrast decreases, the MG applicability range increases. As the dielectric contrast was reduced to 16, the limit shifted to around 5.5% and when it further decreases to 6, the limit shifted to around 7 to 8%. This indicates that for mixing rules to be valid, dielectric contrast should be low enough. Variation in the host material permittivity caused substantial variation in the limit of applicability of the MG mixing rule, while variation in the permittivity of inclusion phase did not affect the limit.

ACKNOWLEDGMENTS

This work was supported through a MURI program sponsored by the Office of Naval Research under Grant No. N000-14-05-1-0541. The authors also gratefully acknowledge the valuable assistance of Mr. Dennis Owsianyck of Integrated Engineering Software.

REFERENCES

- ¹ J.C. Maxwell Garnett, in *Trans. of the Royal Society*, London, 1904, Vol. CCIII, pp. 385-420.
- ² L. K. H. Ven Beck, *Prog. Diel.*, **7**, 71 (1967).
- ³ K. Lichtenecker, *Phys. Z.*, **10**, 1005 (1909).
- ⁴ S. P. Mitoff, *Adv. Mater. Res.*, **3**, 305 (1968).
- ⁵ A. H. Sihvola, *IEEE Trans. Geosci. Rem. Sens.*, **40** [4], 880 (2002).
- ⁶ McCauley J.W., Newnham R. E., and Randall, J. Am. Ceram. Soc., **81**, 979 (1998).
- ⁷ R. Gerson and T.C. Marshall, *J. Appl. Phys.*, **30** [11], 1650 (1959).
- ⁸ C. Baojin, X. Zhou, K. Ren, B. Neese, M. Lin, Q. Wang, F. Bauer, Z. M. Qing, *Science*, **313**, 334 (2006)
- ⁹ J. H. Tortai, N. Bonifaci, A. Denat, *J. Appl. Phys.* **97**, 053304 (2005).
- ¹⁰ T. Kim, J. Nath, J. Wilson, S. Mick, P. D. Franzon, M. B. Steer, and A. I. Kingon, in *Mater. Res. Soc. Symp. Proc.*, **833**, 201 (2005).
- ¹¹ M. Kawasaki, Y. Hara, Y. Yamashiki, N. Asahi, R. Nagase, T. Ueoka, M. Yoshioka, and T. Noaka, in *Proc. 54th Electron. Comp. Tech. Conf.*, **1**, 525 (2004).
- ¹² P.S. Neelakanta, *Handbook of Electromagnetic Materials* (CRC Press, Boca Raton, FL, 1995).
- ¹³ E.F. Kuester and C.L. Holloway, *IEEE Trans. Microw. Theory Techn.*, **3**, 1752-1755 (1990).
- ¹⁴ P. Sheng, *Phys. Rev. Letters*, **45**, 60 (1980).
- ¹⁵ W.T. Doyle and I.S. Jacobs, *J. Appl. Phys.*, **71**, 3926 (1992).
- ¹⁶ R.E. Diaz, W.M. Merrill, and N.G. Alexopoulos, *J. Appl. Phys.*, **84**, 8615 (1998).
- ¹⁷ A. Sihvola, *Electromagnetic Mixing Formulas and Applications* (IEE, London, UK, 1999).
- ¹⁸ M. Y. Koledintseva, J. Wu, J. Zhang, J. L. Drewniak, and K. N. Rozanov, in *Proc. IEEE Symp. Electromag. Compat.*, Santa Clara, CA, 2004, Vol. 1, pp. 309-314.
- ¹⁹ A. Lakhtakia, *Microwave and Optical Technology Letters.*, **17** [4], 276 (1998).
- ²⁰ G. Goodman, R. C. Buchanan, and T. G. Reynolds, III in *Ceramic Materials for Electronics*, 2nd ed. (Marcel Dekker Inc., New York, 1991), pp. 72.
- ²¹ D. A. Payne, in *Tailoring Multiphase and Composite Ceramics*, *Mat. Sci. Res.* **20**, edited by R. E. Tressler et al. (Plenum Press, New York, 1986), pp. 413-431.
- ²² C. Ang, Z. Yu, R. Guo, and A. S. Bhalla, *J. Appl. Phys.*, **93**[6], 3475 (2003).
- ²³ A.Spanoudaki, R. Pelster, *Phys. Rev. B:* **64**, 064205 (2001).
- ²⁴ V. Myroshnychenko and C. Brosseau, *J. Appl. Phys.*, **97**, 044101-14 (2005)
- ²⁵ A. L. An, S. A. Boggs, J. Calame, *IEEE Int. Symp. Elec. Insul.*, 466-469 (2006)
- ²⁶ J. Lopez-Roldan, P. Ozers, T. Judge, C. Rebizant, R. Bosch, and J. Munoz, in *IEEE Int. Symp. Elec. Insul.*, **2**, 685 (1998).
- ²⁷ W. Que and S. A. Sebo, *Proc. Elec./Electron. Insul. Conf.*, 441 (2001).
- ²⁸ A. H. Sihvola, *IEEE Trans. Geosci. Rem. Sens.*, **40** [4], 880 (2002).
- ²⁹ D. A. G. Bruggeman, *Ann. Phys.*, **24**, 636 (1935).
- ³⁰ W.E.Kohler and G.C.Papanicolaou, in *Multiple Scattering and Waves in Random Media*, edited by P.L.Chow, W.E.Kohler, and C.G. Papanicolaou (North-Holland, N.Y., 1981), pp. 199-223.
- ³¹ A. Sihvola and F. Olyslager, *Radio Science*, **31** [6], 1399-1405 (1996).